

# Model free data assimilation with Takens embedding

Ziyi Wang\*      Lijian Jiang†

## Abstract

In many practical scenarios, the dynamical system is not available and standard data assimilation methods are not applicable. Our objective is to construct a data-driven model for state estimation without the underlying dynamics. Instead of directly modeling the observation operator with noisy observation, we establish the state space model of the denoised observation. Through data assimilation techniques, the denoised observation information could be used to recover the original model state. Takens' theorem shows that an embedding of the partial and denoised observation is diffeomorphic to the attractor. This gives a theoretical base for estimating the model state using the reconstruction map. To realize the idea, the procedure consists of offline stage and online stage. In the offline stage, we construct the surrogate dynamics using dynamic mode decomposition with noisy snapshots to learn the transition operator for the denoised observation. The filtering distribution of the denoised observation can be estimated using adaptive ensemble Kalman filter, without knowledge of the model error and observation noise covariances. Then the reconstruction map can be established using the posterior mean of the embedding and its corresponding state. In the online stage, the observation is filtered with the surrogate dynamics. Then the online state estimation can be performed utilizing the reconstruction map and the filtered observation. Furthermore, the idea can be generalized to the nonparametric framework with nonparametric time series prediction methods for chaotic problems. The numerical results show the proposed method can estimate the state distribution without the physical dynamical system.

**keywords:** data assimilation, dynamic mode decomposition, Takens' theorem

## 1 Introduction

Data assimilation (DA) aims to estimate model state for a dynamical system, combining partial and noisy observation with prior information via Bayes's formula [1]. DA has broad applications in various real-world scenarios, such as global positioning systems [2], oil recovery [3], and weather forecasting [4]. Developing practical data assimilation methods for state

---

\*School of Mathematical Sciences, Tongji University, Shanghai 200092, China. (2111156@tongji.edu.cn).

†School of Mathematical Sciences, Tongji University, Shanghai 200092, China. (ljjiang@tongji.edu.cn).

estimation is of practical significance and has attracted great attention from scientists and engineers.

The most popular data assimilation method is Kalman filter [5], proposed by Rudolf Kalman, which provides an exact algorithm to determine the filtering distribution for linear problems with additive Gaussian noise. The basic idea of Kalman filter can be generalized to address nonlinear and non-Gaussian problems. These methods such as extended Kalman filter [6] and ensemble Kalman filter [7], update the model state by a Gaussian assumption. The extended Kalman filter realizes state estimation by linearizing the dynamics. The ensemble Kalman filter (EnKF) generates an ensemble of particles and updates the ensemble by the linear assumption. As approximating Gaussian filters, they may not offer an accurate approximation of the true filtering distribution; nevertheless, they exhibit robustness employing in high dimension [1]. In contrast, as a sequential Monte Carlo method, the particle filter [8] is able to estimate the true filtering distribution in the limit of a large number of particles. However, the particle filter does not perform well in practice because particle degeneracy usually occurs for high-dimension problems. All these classical filtering methods require a specific form of the underlying dynamics, and their performance is significantly contingent upon the underlying dynamical system and model assumptions. In many practical applications, the explicit dynamical system is often unavailable. This motivates us to combine data-driven modeling methods with data assimilation [9–12] for the cases without any physical dynamics.

Data-driven modeling methods have emerged as promising approaches applied to DA, such as dynamic mode decomposition (DMD) [13–15], sparse identification of nonlinear dynamical systems (SINDy) [16], etc. When the transition model is unknown, these techniques offer an effective surrogate for the transition operator and enable the successful execution of DA within the underlying dynamic system [17]. When the observation operator is identical, the method proposed by [18] can effectively denoise the model state by offering a proxy transition model with DMD. Kalman-Takens method [19] models the transition operator in the scenarios where only partial state data is available. This approach is based on Takens’ theorem [20, 21], which shows that a time-delayed embedding of partial and denoised observation is diffeomorphic to the attractor of a compact manifold. Furthermore, the research in [22] has shown that the mapping from a time-delayed embedding to the attractor can be effectively learned to reconstruct the true model state using supervised learning techniques, such as neural networks (NNs). However, certain limitations exist within the current research. For instance, the Kalman-Takens method [19] is unable to estimate the unobservable state variables. The methodology proposed in [22] requires noise-free observation data, which limits its applicability in the scenarios where observation data is inherently noisy.

In this paper, we propose a method, DMD-Takens based EnKF (DMD-T EnKF), which facilitates real-time estimation with data-driven modeling methods in the case where the underlying dynamical system and noise information are unknown. Considering the challenges in directly modeling the observation operator, we establish the state space model of the denoised observation. The denoised observation is then estimated with DA. This allows us to estimate the model state utilizing the embedding of the denoised observations through a reconstruction map based on Takens’ theorem. In the offline stage, we firstly construct the surrogate transition model for the denoised observation by DMD with noisy observations. Given the transition model, the filtering distribution of the denoised observation is estimated

by adaptive ensemble Kalman filter (adaptive EnKF) [23], without knowledge of the model error and observation noise covariances. The posterior mean of the denoised observation will be leveraged to construct a more accurate transition model. Besides, the filtering distribution of the time-delayed embedding can be approximated with the denoised observations. Consequently, we learn the reconstruction map through supervised learning methods, utilizing the posterior mean of the embedding and its corresponding model state data. In the online stage, we estimate the denoised observation by adaptive EnKF and construct time-delayed coordinate vector. After that, the filtering distribution of model state is approximated with posterior samples obtained from the reconstruction map. Furthermore, our method can be extended to a nonparametric framework: KNN-Takens based EnKF (KNN-T EnKF). The transition model in the denoised observation space, along with the reconstruction map is learned using nonparametric time series prediction methods for chaotic problems [24–26]. Compared with Kalman-Takens method [19], our method can estimate all the model state through the reconstruction map.

The paper is organized as follows. Section 2 provides a brief overview of EnKF. In Section 3, we present the construction of surrogate model in the offline stage and provide an online inference approach. In Section 4, a nonparametric framework is introduced for online state estimation. In Section 5, we present several numerical examples to approximate the filtering distribution without the underlying dynamics. The paper concludes with a summary in Section 6.

## 2 Preliminaries

Let us consider the dynamical system governed by the map  $\Phi \in C(\mathbb{R}^n, \mathbb{R}^n)$  with noisy observation  $y = \{y_k\}_{k \in N}$  depending on the observation operator  $h \in C(\mathbb{R}^n, \mathbb{R}^m)$ ,

$$\begin{cases} x_{k+1} = \Phi(x_k) + \xi, & x_0 \sim N(m_0, C_0), \\ y_{k+1} = h(x_{k+1}) + \eta, & k \in N, \end{cases} \quad (2.1)$$

where  $\xi \sim \mathcal{N}(0, Q)$  and  $\eta \sim \mathcal{N}(0, R)$ . Data assimilation is concerned with two fundamental issues: smoothing and filtering. In this paper, our focus is specifically on the filtering problem. We firstly introduce EnKF [7], which can effectively determine the filtering distribution for nonlinear and non-Gaussian problems by a Gaussian assumption.

Let  $Y_k := \{y_\tau\}_{\tau=1}^k$  represent the accumulated observation data up to time step  $k$ . EnKF comprises two essential steps: prediction and analysis for evaluating filtering distribution  $p(x_{k-1}|Y_{k-1}) \rightarrow p(x_k|Y_k)$ . Let  $\{x_{k-1}^{a,1}, \dots, x_{k-1}^{a,N}\}$  be the samples drawn from the filtering distribution  $p(x_{k-1}|Y_{k-1})$ , which is approximated by

$$p(x_{k-1}|Y_{k-1}) \approx \frac{1}{N} \sum_{n=1}^N \delta_{(x_{k-1}^{a,n})}(x_{k-1}),$$

where  $\delta$  is the Dirac delta function and  $N$  denotes the ensemble size. For the prediction step, we can apply the transition model to obtain the ensembles and approximate the prediction

distribution at time  $k$ :

$$\begin{aligned}
p(x_k|Y_{k-1}) &= \int p(x_k, x_{k-1}|Y_{k-1})dx_{k-1} \\
&= \int p(x_k|x_{k-1})p(x_{k-1}|Y_{k-1})dx_{k-1} \\
&\approx \frac{1}{N} \sum_{n=1}^N \mathcal{N}(x_k|\Phi(x_{k-1}^{a,n}), Q) \\
&\approx \frac{1}{N} \sum_{n=1}^N \delta_{(x_k^{f,n})}(x_k),
\end{aligned} \tag{2.2}$$

where  $x_k^{f,n} = \Phi(x_{k-1}^{a,n}) + \xi_k$  represents the samples drawn from the prediction distribution  $p(x_k|Y_{k-1})$ .

In the analysis step, according to Bayes' rule, the filtering distribution at time  $k$  satisfies

$$p(x_k|Y_k) \propto p(y_k|x_k)p(x_k|Y_{k-1}) \approx \frac{1}{N} \sum_{n=1}^N \mathcal{N}(y_k|h(x_k), R)\mathcal{N}(x_k|\Phi(x_{k-1}^{a,n}), Q).$$

If the observation operator is linear, the mixture of Gaussians  $p(x_k|Y_{k-1})$  in (2.2) is approximated by a single Gaussian distribution. Consequently, the posterior distribution can be approximated by a Gaussian distribution,

$$p(x_k|Y_k) \propto p(y_k|x_k)p(x_k|Y_{k-1}) \approx \mathcal{N}(y_k|Hx_k, R)\mathcal{N}(x_k|x_k^f, \hat{\Sigma}_k),$$

where  $H$  is the linear observation operator,  $x_k^f = \frac{1}{N} \sum_{n=1}^N x_k^{f,n}$ ,  $\hat{\Sigma}_k = \frac{1}{N-1} \sum_{n=1}^N (x_k^{f,n} - x_k^f)(x_k^{f,n} - x_k^f)^T$ . The main steps of EnKF read as following,

$$\begin{aligned}
\hat{K} &= \hat{\Sigma}_k H^T (H \hat{\Sigma}_k H^T + R)^{-1}, \\
x_k^{a,n} &= x_k^{f,n} + \hat{K}(y_k - y_k^n), \\
y_k^n &= H x_k^{f,n} + \eta_k^n, \\
x_k^a &= \frac{1}{N} \sum_{n=1}^N x_k^{a,n},
\end{aligned}$$

where  $x_k^a$  denotes the posterior mean and  $y_k^n$  represents a pseudo-observation with  $\eta_k^n \sim \mathcal{N}(0, R)$ . If the noise statistics  $Q$  and  $R$  are unavailable, adaptive EnKF [23] utilizes the cross-correlations of innovations to estimate them. This method can realize state estimation in the absence of noise statistics.

We can find that EnKF relies on the explicit form of the transition operator  $\Phi$  and observation operator  $h$ . In many practical scenarios, the dynamical system (2.1) is unavailable and standard algorithms are not applicable. Instead, we can obtain trajectories from historical observations or numerical simulations. Therefore, without the underlying dynamics, our goal is to realize online state estimation using a labeled dataset  $\{x_k^{(i)}, y_k^{(i)}\}_{k=1}^T, i = 1, 2, \dots, M$ , where  $k$  denotes the time index and  $i$  represents the  $i$ -th trajectory.

### 3 DMD-Takens based EnKF

In this section, we describe DMD-Takens based EnKF, which can provide state estimation without knowledge of the underlying dynamics. Based on Takens' theorem, we estimate the denoised observation with DA and learn the reconstruction map via a supervised learning method. This method includes two stages: the offline stage and the online stage. We will present the basic framework of the proposed approach and the details of the two stages.

#### 3.1 Basic framework

Instead of directly modeling the original dynamics as specified in (2.1), we establish a state space model of the denoised observation. The model state  $x_k$  can be estimated through the reconstruction map derived from Takens' theorem.

In our context, the denoised observation is represented by  $\hat{y}_k$ . Assuming that the evolution process of  $\hat{y}_k$  is Markovian, the discrete-time dynamical system for  $\hat{y}_k$  is defined by

$$\begin{cases} \hat{y}_{k+1} = f(\hat{y}_k) + \omega_k, \\ y_{k+1} = \hat{y}_{k+1} + \eta_{k+1}, \end{cases} \quad (3.3)$$

where  $f$  is the transition model, and  $\omega = \{\omega_k\}_{k \in N}$  represents model error, which is assumed as an i.i.d sequence. In this section, we employ DMD to construct the surrogate transition model for  $\hat{y}_k$ . DMD [13–15] is a data-driven modeling method and numerically approximates the Koopman operator in a finite-dimensional space. We assume that this space is spanned by a set of observables, represented as  $\Psi = \{\psi_1, \psi_2, \dots, \psi_m, \dots, \psi_{N_k}\}$ . The first  $m$  components  $\{\psi_1, \dots, \psi_m\}$  is assumed as  $m$  scalar-valued functions containing the full-state observable  $g(\hat{y}) = \hat{y}$ , i.e.,

$$\psi_i(\hat{y}) = \mathbf{e}_i^T \hat{y}, \quad i = 1, 2, \dots, m,$$

where  $\mathbf{e}_i$  is the  $i$ -th unit vector in  $\mathbb{R}^m$ . Then we define the data matrices  $\hat{Y}_0$  and  $\hat{Y}_1$  as follows,

$$\begin{aligned} \hat{Y}_0 &:= [\Psi(\hat{y}_1), \dots, \Psi(\hat{y}_{l-1})], \\ \hat{Y}_1 &:= [\Psi(\hat{y}_2), \dots, \Psi(\hat{y}_l)], \end{aligned}$$

where  $l$  represents the serial number of snapshots. DMD aims to compute the matrix  $K$ , which approximates the Koopman operator in the sense of least-squares,

$$K = \arg \min_{\tilde{K}} \|\hat{Y}_1 - \tilde{K}\hat{Y}_0\|_F,$$

where  $\|\cdot\|_F$  represents the Frobenius norm. The best-fit matrix can be computed by  $K = \hat{Y}_1 \hat{Y}_0^\dagger$ , where  $\dagger$  is the Moore-Penrose inverse. The transition model  $f$  is then approximated by the first  $m$  rows of  $K$ , denoted as  $K^y$ . Consequently, the dynamics of  $\hat{y}_k$  can be approximated as follows,

$$\begin{cases} \hat{y}_{k+1} = K^y \Psi(\hat{y}_k) + \hat{\omega}_k, \\ y_{k+1} = \hat{y}_{k+1} + \eta_{k+1}, \end{cases} \quad (3.4)$$

where  $\hat{\omega}_k = f(\hat{y}_k) - K^y \Psi(\hat{y}_k) + \omega_k$  includes two primary components: the approximation error of  $f(\hat{y}_k) - K^y \Psi(\hat{y}_k)$  and model error  $\omega_k$ , which is assumed to satisfy  $\hat{\omega}_k \sim \mathcal{N}(0, M)$ .

The calculation of  $K^y$  will be described in the following subsection. If  $K^y$  is available, the filtering distribution  $p(\hat{y}_k|Y_k)$  can be estimated with adaptive EnKF, which can adaptively estimate the noise statistics  $M$  and  $R$ . Then we aim to evaluate the filtering distribution  $p(x_k|Y_k)$  of the model state through the denoised observation.

*Remark 3.1.* The transition model is constructed using DMD or SINDy.

When the observation is partial, the information in  $\hat{y}_k$  is inadequate to accurately estimate the model state  $x_k$ .

**Theorem 3.1.** [Takens, 1981] *Let  $M$  be a compact manifold of dimension  $m$ . For pairs  $(\varphi, g)$ , where  $\varphi : M \rightarrow M$  is a smooth (at least  $C^2$ ) diffeomorphism and  $g : M \rightarrow \mathbb{R}$  a smooth function, it is a generic property that the  $(2m + 1)$ - delay observation map  $\mathcal{G}_{(\varphi, g)} : M \rightarrow \mathbb{R}^{2m+1}$  given by*

$$\mathcal{G}_{(\varphi, g)}(z) = (g(z), g \circ \varphi(z), \dots, g \circ \varphi^{2m}(z))$$

*is an embedding.*

This theorem can be extended to the case of vector observations [21]. If  $\varphi = \Phi^\dagger$ ,  $g = h$ , we have

$$\mathcal{G}_{(\varphi, g)}(x_k) = (\hat{y}_k, \hat{y}_{k-1}, \dots, \hat{y}_{k-2m}).$$

Based on Takens' theorem, we can construct the embedding  $\mathcal{G}_{(\varphi, g)}(x_k)$  and estimate the model state  $x_k$  via a reconstruction map. For convenience, we denote the embedding as  $\mathbf{y}_k := (\hat{y}_k, \hat{y}_{k-1}, \dots, \hat{y}_{k-d+1})$ , where  $d$  represents the time-delay length and can be determined by the false nearest neighbors methods [27, 28]. The reconstruction map is defined as:

$$x_k = F(\mathbf{y}_k, \theta), \quad F : \mathbb{R}^{d \times m} \rightarrow \mathbb{R}^n,$$

where  $\theta$  represents the parameters of this map. We can estimate  $p(x_k|Y_k)$  using samples drawn from  $p(\mathbf{y}_k|Y_k)$  via the map  $F$ . Moreover, if  $p(\mathbf{y}_k|Y_k)$  can be accurately evaluated, we can accurately estimate the filtering distribution  $p(x_k|Y_k)$  with a large number of samples, i.e.,

$$\begin{aligned} p(x_k|Y_k) &= \frac{\int p(x_k, \mathbf{y}_k, Y_k) d\mathbf{y}_k}{p(Y_k)} \\ &= \frac{\int p(x_k|\mathbf{y}_k)p(\mathbf{y}_k, Y_k) d\mathbf{y}_k}{p(Y_k)} \\ &= \int p(x_k|\mathbf{y}_k)p(\mathbf{y}_k|Y_k) d\mathbf{y}_k \\ &\approx \sum_{j=1}^{N'} p(x_k|\mathbf{y}_k^j) \\ &= \sum_{j=1}^{N'} \delta_{F(\mathbf{y}_k^j, \theta)}(x_k), \end{aligned}$$

where  $\mathbf{y}_k^j$  represents the  $j$ -th sample drawn from  $p(\mathbf{y}_k|Y_k)$ ,  $j = 1, 2, \dots, N'$ . We will show that the filtering distribution  $p(\mathbf{y}_k|Y_k)$  can be approximated by the distribution  $p(\hat{y}_k|Y_k)$  in the following section. The general framework of our approach is described in Fig. 3.1. We aim to model the surrogate transition model  $K^y$  and the reconstruction map  $F$  for online estimation.

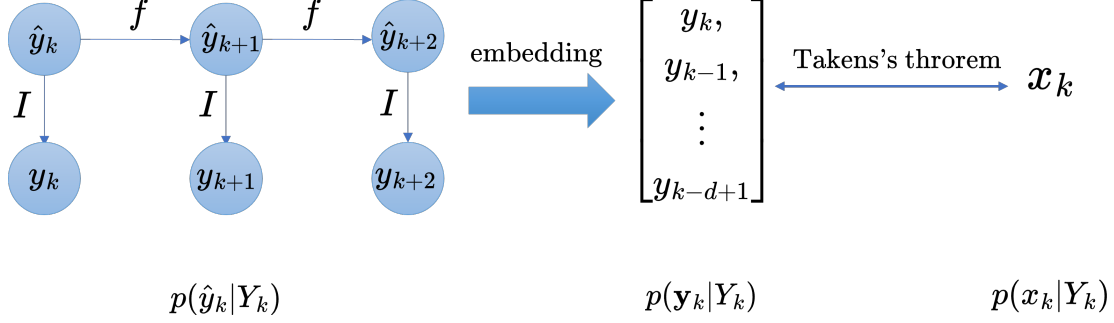


Figure 3.1: The general framework for DMD-Takens based EnKF.

### 3.2 Offline data-driven modeling

In this stage, we learn the surrogate transition model  $K^y$  and the reconstruction map  $F$  with the labeled dataset  $\{x_k^{(i)}, y_k^{(i)}\}_{k=1}^T$ .

Inspired by EnKF-DMD in [18], the observation operator can be considered as identical. The DMD matrix  $K^y$  can be initialized using noisy snapshots  $\{y_1^{(i)}, \dots, y_T^{(i)}\}_{i=1}^M$ , which are denoted by  $K^{y,(0)}$ . For simplicity of notations, the subscript  $i$  will be suppressed in the rest of paper because the method keeps the same for each trajectory. Accordingly, the adaptive EnKF is employed to estimate the filtering distribution  $p(\hat{y}_k|Y_k, K^{y,(0)})$  and generate the posterior ensemble  $\{\hat{y}_k^{a,1}, \dots, \hat{y}_k^{a,N}\}$ , thereby facilitating noise reduction in the observation data. Subsequently, the posterior mean data set, denoted as  $\{\hat{y}_1^a, \dots, \hat{y}_T^a\}$ , is utilized to construct a more refined transition model  $K^{y,(1)}$ . In practice, this process can be applied iteratively to derive  $K^{y,(t)}, t \geq 2$ . This iterative process will be elucidated from the perspective of the expectation-maximization (EM) algorithm in Section 3.4.

Then we estimate the delay coordinate vector  $\mathbf{y}_k$  through the estimates of  $\{\hat{y}_k, \dots, \hat{y}_{k-d+1}\}$ . The filtering distribution of  $p(\mathbf{y}_k|Y_k)$  satisfies

$$p(\hat{y}_k, \dots, \hat{y}_{k-d+1}|Y_k) = \underbrace{p(\hat{y}_{k-d+1}|Y_k)}_{\text{I}} \prod_{i=0}^{d-2} \underbrace{p(\hat{y}_{k-i}|\hat{y}_{k-i-1}, Y_k)}_{\text{II}}, \quad (3.5)$$

where I and II represent the conditional distribution of  $\hat{y}_{k-d+1}$  and  $\hat{y}_{k-i}$  given the data sets  $\{Y_{k-d+1}, y_{k-d+2}, \dots, y_k\}$  and  $\{\hat{y}_{k-i-1}, Y_{k-i}, y_{k-i+1}, \dots, y_k\}$ , respectively. We assume that  $Y_{k-d+1}$  and  $\{\hat{y}_{k-i-1}, Y_{k-i}\}$  retain sufficient information for reliable analysis. Therefore, the distributions  $p(\hat{y}_{k-d+1}|Y_{k-d+1})$  and  $p(\hat{y}_{k-i}|\hat{y}_{k-i-1}, Y_{k-i})$  are employed to approximate I and II, separately.

To sample from (3.5), we firstly sample from the filtering distribution  $p(\hat{y}_{k-d+1}|Y_{k-d+1})$ . The posterior ensemble  $\{\hat{y}_{k-d+1}^{a,1}, \dots, \hat{y}_{k-d+1}^{a,N}\}$  is available from the previous process. Then we sample from  $p(\hat{y}_{k-d+2}|\hat{y}_{k-d+1}^{a,j}, Y_{k-d+2}), j = 1, 2, \dots, N$ , which satisfies

$$\begin{aligned} p(\hat{y}_{k-d+2}|\hat{y}_{k-d+1}^{a,j}, Y_{k-d+2}) &= p(\hat{y}_{k-d+2}|\hat{y}_{k-d+1}^{a,j}, y_{k-d+2}) \\ &\propto p(\hat{y}_{k-d+2}|\hat{y}_{k-d+1}^{a,j})p(y_{k-d+2}|\hat{y}_{k-d+1}^{a,j}). \end{aligned}$$

The particle  $\hat{y}_{k-d+2}^{a,j}$  is generated using adaptive EnKF and can be considered as a sample from the distribution  $p(\hat{y}_{k-d+2}|\hat{y}_{k-d+1}^{a,j}, Y_{k-d+2})$ . We can recursively sample from the distribution

$p(\hat{y}_{k-i}|\hat{y}_{k-i-1}^{a,j}, Y_{k-i})$ ,  $i = d - 3, \dots, 0$ . The trajectory

$$\mathbf{y}_k^{a,j} := \{\hat{y}_{k-d+1}^{a,j}, \dots, \hat{y}_k^{a,j}\} \quad (3.6)$$

can be regarded as a sample drawn from the joint pdf  $p(\mathbf{y}_k|Y_k)$ , i.e.,

$$p(\mathbf{y}_k|Y_k) \approx \frac{1}{N} \sum_{j=1}^N \delta_{\mathbf{y}_k^{a,j}}(\mathbf{y}_k).$$

The sampling process of  $p(\mathbf{y}_k|Y_k)$  is depicted in Fig. 3.2.

The posterior mean  $\mathbf{y}_k^a$  can be seen as maximum a posterior (MAP) estimation of the truth  $\mathbf{y}_k$ . We can utilize the dataset  $\{x_k^{(i)}, \mathbf{y}_k^{a,(i)}\}_{k=1}^T$  to learn the reconstruction map  $F$  with supervised learning methods. This map can be approximated with parametric methods, such as fully connected neural networks, radial basis function network, etc. The following is the loss function to learn the reconstruction map  $F$ ,

$$\mathcal{L}_F = \frac{1}{MT} \sum_{i=1}^M \sum_{k=1}^T \|x_k^{(i)} - F(\mathbf{y}_k^{a,(i)}, \theta)\|_2^2.$$

We can also learn the reconstruction map with nonparametric methods, which will be described in the following section. The general framework to construct the surrogate model is described in Algorithm 1.

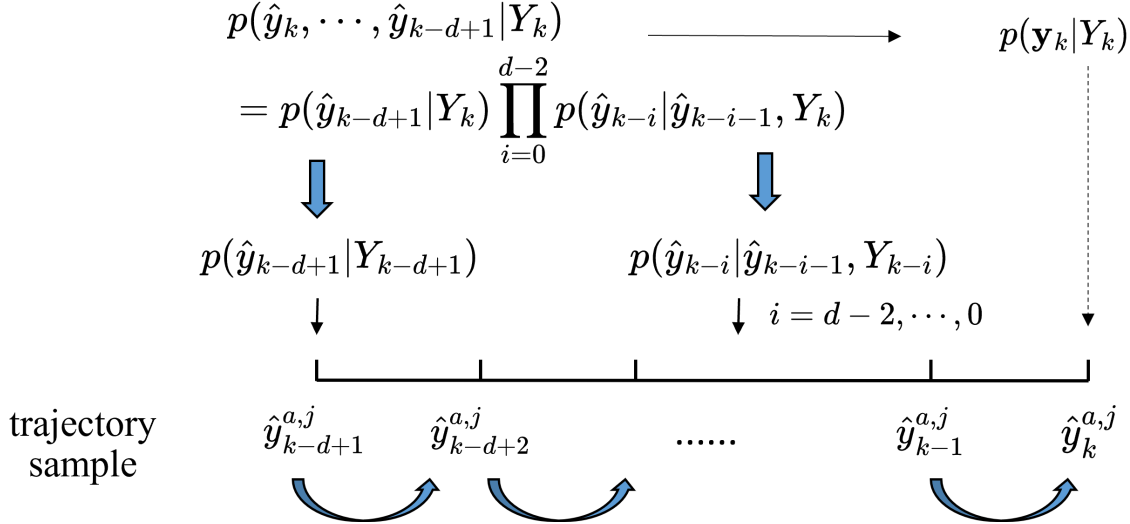


Figure 3.2: The sampling process for  $p(\mathbf{y}_k|Y_k)$ .

### 3.3 Online estimation

The surrogate model can be utilized for real-time estimation. Given the proxy transition model  $K^{y,(t)}$ , we compute the posterior distribution  $p(\hat{y}_k|Y_k)$  with adaptive EnKF. Then the samples of  $\mathbf{y}_k$  are collected with the trajectories  $\{\mathbf{y}_k^{a,1}, \dots, \mathbf{y}_k^{a,N}\}$  defined in (3.6). We can

---

**Algorithm 1** DMD-Takens based EnKF: construction of the surrogate model
 

---

**Input:** labeled dataset  $\{x_k^{(i)}, y_k^{(i)}\}_{k=1}^T, i = 1, 2, \dots, M$

**Output:** transition model  $K^y$ , reconstruction map  $F$

1: Estimate  $K^y$  and the distribution  $p(\hat{y}_k|Y_k)$ . The initial DMD matrix  $K^{y,(0)}$  is calculated by  $\{y_1^{(i)}, \dots, y_T^{(i)}\}_{i=1}^M$ .

(i): calculate  $p(\hat{y}_k^{(i)}|Y_k, K^{y,(t)})$  and obtain the posterior ensemble  $\{\hat{y}_k^{a,1,(i)}, \dots, \hat{y}_k^{a,N,(i)}\}$  with adaptive EnKF.

(ii): update the DMD matrix  $K^{y,(t+1)}$ . Let

$$\begin{aligned} Y_0^a &:= [\hat{y}_1^{a,(1)}, \dots, \hat{y}_{T-1}^{a,(1)}, \dots, \hat{y}_1^{a,(M)}, \dots, \hat{y}_{T-1}^{a,(M)}], \\ Y_1^a &:= [\hat{y}_2^{a,(1)}, \dots, \hat{y}_T^{a,(1)}, \dots, \hat{y}_2^{a,(M)}, \dots, \hat{y}_T^{a,(M)}], \end{aligned}$$

we can obtain the matrix  $K^{(t+1)} = \Psi(Y_1^a)\Psi(Y_0^a)^\dagger$ . Then  $K^{y,(t+1)}$  is available with the first  $m$  rows of the DMD matrix  $K^{(t+1)}$ .

2: Construct the sample  $\mathbf{y}_k^{a,j,(i)} := \{\hat{y}_{k-d+1}^{a,j,(i)}, \dots, \hat{y}_k^{a,j,(i)}\}$ , i.e.,

$$p(\mathbf{y}_k^{(i)}|Y_k) = \frac{1}{N} \sum_{j=1}^N \delta_{\mathbf{y}_k^{a,j,(i)}}(\mathbf{y}_k).$$

3: Learn the reconstruction map  $F$  utilizing the dataset  $\{x_k^{(i)}, \mathbf{y}_k^{a,(i)}\}_{k=1}^T$  with NNs by minimizing the loss function:

$$\mathcal{L}_F = \frac{1}{MT} \sum_{i=1}^M \sum_{k=1}^T \|x_k^{(i)} - F(\mathbf{y}_k^{a,(i)}, \theta)\|_2^2.$$


---

get the samples  $\{x_k^{a,1}, \dots, x_k^{a,N}\}$  from the corresponding samples  $\{\mathbf{y}_k^{a,1}, \dots, \mathbf{y}_k^{a,N}\}$  through the reconstruction map  $F$ , and approximate the distribution  $p(x_k|Y_k)$  by

$$p(x_k|Y_k) \approx \frac{1}{N} \sum_{j=1}^N \delta_{x_k^{a,j}}(x_k).$$

The prediction accuracy of  $K^{y,(t)}$  may decrease for long-time prediction. To address this challenge, we update the DMD matrix with new observation in a new time window. Assuming that the DMD matrix varies with time, denoted by  $K_k$ , the initial  $K_0$  is assigned as  $K^{(t)}$ . The filtering distribution of  $p(K_k|Y_k)$  satisfies

$$\begin{aligned} p(K_k|Y_k) &= \int p(K_k, \hat{y}_{1:k}|Y_k) d\hat{y}_{1:k} \\ &= \int p(K_k|\hat{y}_{1:k}) p(\hat{y}_{1:k}|y_{1:k}) d\hat{y}_{1:k} \\ &\approx p(K_k|\hat{y}_{1:k}^a), \end{aligned}$$

where the smooth distribution  $p(\hat{y}_{1:k}|y_{1:k})$  is approximated by the posterior mean  $\{\hat{y}_1^a, \dots, \hat{y}_k^a\}$ . We set the fixed-length time window  $\{\hat{y}_{k-T+1}, \dots, \hat{y}_k\}$  to update  $K_k$ , i.e.,

$$p(K_k|y_{k-T+1:k}) \approx p(K_k|\hat{y}_{k-T+1:k}^a),$$

where  $T$  represents the length of time window.

According to the definition of  $\Psi(\hat{y}_k)$ , we have

$$\Psi(\hat{y}_{k+1}) = K\Psi(\hat{y}_k) + \hat{\Omega}_k,$$

where  $\hat{\Omega}_k \sim \mathcal{N}(0, \hat{M}_k)$  represents the model error between  $\Psi(\hat{y}_{k+1})$  and  $\Psi(\hat{y}_k)$ . We denote

$$\begin{aligned} Y_{k-T+1:k-1}^a &:= [\hat{y}_{k-T+1}^a, \dots, \hat{y}_{k-1}^a], \\ Y_{k-T+2:k}^a &:= [\hat{y}_{k-T+2}^a, \dots, \hat{y}_k^a], \\ \hat{\Omega}_{k-T+1:k-1} &:= [\hat{\Omega}_{k-T+1}, \dots, \hat{\Omega}_{k-1}], \end{aligned}$$

and then get

$$\Psi(Y_{k-T+2:k}^a) = K_k\Psi(Y_{k-T+1:k-1}^a) + \Omega_{k-T+1:k-1}.$$

We aim to obtain the least-squares estimate of  $K_k$  by minimizing the following problem,

$$K_k = \arg \min_{\tilde{K}} \|\Psi(Y_{k-T+2:k}^a) - \tilde{K}\Psi(Y_{k-T+1:k-1}^a)\|_F.$$

Then the DMD matrix  $K_k$  is updated using the formula,

$$K_k = \Psi(Y_{k-T+2:k}^a)\Psi(Y_{k-T+1:k-1}^a)^\dagger.$$

Compared with the previous section, we update the DMD matrix in temporal space instead of the physical space to keep high accuracy for long-time prediction. The main steps of this algorithm are shown in Algorithm 2.

---

**Algorithm 2** Online estimation with the proxy model

---

**Input:** observation  $y_k$  and  $K_0$

**Output:** posterior  $p(x_k|Y_k)$

- 1: Estimate  $p(\hat{y}_k|Y_k, K_{k-1})$  with adaptive EnKF and collect the samples of  $\mathbf{y}_k$ .
- 2: Estimate the posterior  $p(x_k|Y_k)$  with the reconstruction map  $F$ :

$$p(x_k|Y_k) = \frac{1}{N} \sum_{j=1}^N \delta_{F(\mathbf{y}_k^j, \theta)}(x_k).$$

- 3: Update  $K_k$  with  $K_k = \Psi(Y_{k-T+2:k}^a)\Psi(Y_{k-T+1:k-1}^a)^\dagger$  at predetermined time intervals.
- 

### 3.4 From EM perspective

In this section, we develop an iterative process to build the transition model  $K^{y,(t)}$  from the perspective of EM algorithm. Denoting time-varying noise statistics as  $M_k$  and  $R_k$ , our

objective is to determine the maximum likelihood estimation for  $K^y$ . Since  $K^y$  is determined by  $K$ , we concentrate on deriving the solution for  $K$ . The cost function can be derived by

$$\mathcal{J}(K) = -\log p(y_{1:T}|K) = -\log \int p(y_{1:T}, z_{1:T}|K) dz_{1:T},$$

where  $z_k = \Psi(\hat{y}_k)$  is the latent variable, and  $z_{1:T} = \{\Psi(\hat{y}_k)\}_{k=1}^T$ . The optimization of this loss function can be achieved with EM algorithm.

The initial DMD matrix  $K^{(0)}$  can be calculated with the noisy observations. In the E step, it is essential to evaluate the distribution  $p(z_{1:T}|y_{1:T}, K^{y,(t)})$ . To improve the computational efficiency, the filtering distribution is utilized to approximate the smooth distribution  $p(z_{1:T}|y_{1:T}, K^{(t)})$ . Given the transition model  $K^{y,(t)}$ , the posterior mean  $\hat{y}_k^a$  can be obtained using adaptive EnKF.

In the M step, our goal is to minimize

$$\mathcal{J}(K) = -\int p(z_{1:T}|y_{1:T}, K^{(t)}) \log p(y_{1:T}, z_{1:T}|K) dz_{1:T}.$$

We approximate  $p(z_{1:T}|y_{1:T}, K^{(t)})$  with the posterior mean trajectory  $\{\Psi(\hat{y}_k^a)\}_{k=1}^T$  and get

$$\mathcal{J}(K) \approx -\log p(y_{1:T}, z_{1:T}^a|K),$$

where  $z_{1:T}^a = \{\Psi(\hat{y}_k^a)\}_{k=1}^T$ . According to the form of (3.4), we can define the dynamical system of  $\Psi(\hat{y}_k)$  by

$$\begin{cases} \Psi_{k+1} = K\Psi_k + \hat{\Omega}_k, \\ y_{k+1} = \tilde{h}(\Psi_k) + \eta_{k+1}, \end{cases} \quad (3.7)$$

where  $\Psi_k := \Psi(\hat{y}_k)$ . The observation operator  $\tilde{h}$  contains the first  $m$  components of  $\Psi_k$  and

$$\tilde{h}(\Psi_k) = \begin{bmatrix} \Psi_{k,1} \\ \vdots \\ \Psi_{k,m} \end{bmatrix}.$$

Then according to (3.7), we can transfer  $\mathcal{J}(K)$  into

$$\begin{aligned} \mathcal{J}(K) &\approx -\log p(y_{1:T}, \Psi_{1:T}^a|K) \\ &\approx -\sum_{k=2}^T \log p(\Psi_k^a|\Psi_{k-1}^a) - \sum_{k=1}^T \log p(y_k|\Psi_k^a) - \log p(\Psi_1^a) \\ &\approx \frac{1}{2} \sum_{k=2}^T \{\|\Psi_k^a - K\Psi_{k-1}^a\|_{\hat{M}_k^{-1}}^2 + \log |\hat{M}_k| + N_k \log(2\pi)\} - \log p(\Psi_1^a) \\ &+ \frac{1}{2} \sum_{k=1}^T \{\|y_k - \tilde{h}(\Psi_k^a)\|_{R_k^{-1}}^2 + \log |R_k| + m \log(2\pi)\} \\ &\approx \frac{1}{2} \sum_{k=2}^T \|\Psi_k^a - K\Psi_{k-1}^a\|_{\hat{M}_k^{-1}}^2 + \dots \end{aligned}$$

where  $\Psi_k^a := \Psi(\hat{y}_k^a)$ . Except for the first term, the rest terms are not related to  $K$ . We denote the data matrices as

$$\begin{aligned} Y_0^a &:= [\hat{y}_1^a, \dots, \hat{y}_{T-1}^a], \\ Y_1^a &:= [\hat{y}_2^a, \dots, \hat{y}_T^a]. \end{aligned}$$

If we approximate the norm  $\|\Psi_k^a - K\Psi_{k-1}^a\|_{\hat{M}_k^{-1}}$  with the Frobenius norm  $\|\Psi_k^a - K\Psi_{k-1}^a\|_F$ , the cost function can be approximated as follows:

$$\mathcal{J}(K) \approx \min_K \|\Psi(Y_1^a) - K\Psi(Y_0^a)\|_F^2.$$

The DMD matrix  $K$  can be updated with  $K^{(t+1)} = \Psi(Y_1^a)\Psi(Y_0^a)^\dagger$ .

## 4 KNN-Takens based EnKF

In this section, we present a nonparametric approach, namely KNN-Takens based EnKF, which employs analog forecasting strategies for online estimation. Compared with DMD-T EnKF, the transition model  $f$  of  $\hat{y}_k$  and the reconstruction map  $F$  are constructed with nonparametric time series prediction methods for chaotic time series problems [19, 24, 25].

In the offline stage, we consider constructing the proxy model for  $f$  and denoise the observations. Based on the existing diffeomorphism from Takens' theorem, we embed the partial observation and utilize K-nearest neighbors (KNN) method for prediction. Given the posterior sample  $\mathbf{y}_k^{a,j} = \{\hat{y}_k^{a,j}, \dots, \hat{y}_{k-d+1}^{a,j}\}$ , we locate its  $M$  nearest neighbors

$$\{y_{k'}, \dots, y_{k'-d+1}\}, \{y_{k''}, \dots, y_{k''-d+1}\}, \dots, \{y_{k^M}, \dots, y_{k^M-d+1}\}$$

within the library of historical data with respect to Euclidean distance. The known successors  $\{y_{k'+1}, y_{k''+1}, \dots, y_{k^M+1}\}$  are used to predict the prior sample  $\hat{y}_{k+1}^{f,j}$ . Several analog forecasting operators are available, such as the locally constant analog operator (L-C operator) and the locally weighted linear regression operator (L-L operator) [19, 26]. These operators are defined as follows:

- L-C operator:

$$f_{\text{LC}}(\mathbf{y}_k^{a,j}) = w_1 y_{k'+1} + w_2 y_{k''+1} + \dots + w_M y_{k^M+1},$$

where  $w_1, w_2, \dots, w_M$  are weights that determine the contribution of each neighbor in constructing the prediction. The simplest form of weights is given by  $w_1 = w_2 = \dots = w_M = \frac{1}{M}$  and can be further defined as the normalized kernel function:

$$w_i[\mathbf{y}_k^{a,j}] = \frac{g(\mathbf{y}_k^{a,j}, \mathbf{y}^{(i)})}{\sum_{i=1}^M g(\mathbf{y}_k^{a,j}, \mathbf{y}^{(i)})},$$

where  $\mathbf{y}^{(i)}$  represents the  $i$ -th nearest neighbor of  $\mathbf{y}_k^{a,j}$  with  $g(u, v) = \exp(-\lambda\|u - v\|^2)$ .

- L-L operator: fit a weighted linear regression between  $\{\mathbf{y}_{k'}^{a,j}, \mathbf{y}_{k''}^{a,j}, \dots, \mathbf{y}_{k^M}^{a,j}\}$  and the corresponding successors  $\{y_{k'+1}, y_{k''+1}, \dots, y_{k^M+1}\}$ , where the weights are defined as the above content. We can calculate the regression slope  $\theta(\mathbf{y}_k^{a,j})$  and intercept  $\phi(\mathbf{y}_k^{a,j})$  using weighted least squares estimates. The L-L operator is written as

$$f_{\text{LL}}(\mathbf{y}_k^{a,j}) = \theta(\mathbf{y}_k^{a,j})\mathbf{y}_k^{a,j} + \phi(\mathbf{y}_k^{a,j}).$$

With the analog forecasting operators, the dynamical system can be approximated as follows:

$$\begin{cases} \hat{y}_{k+1} = f_{\text{LC/LL}}(\mathbf{y}_k) + \hat{\omega}_k, \\ y_{k+1} = \hat{y}_{k+1} + \eta_{k+1}. \end{cases}$$

Then the posterior distribution  $p(\hat{y}_{k+1}|Y_{k+1})$  can be estimated with adaptive EnKF. We construct the set  $\mathcal{Y} = \{\mathbf{y}_d^{a,(i)}, \dots, \mathbf{y}_T^{a,(i)}\}_{i=1}^M$ , which comprises the posterior mean of  $\mathbf{y}_k$  from the training labeled dataset. The ensemble of corresponding model state is assigned as  $\mathcal{X} = \{x_d^{(i)}, \dots, x_T^{(i)}\}_{i=1}^M$ . The two sets will be utilized to learn the reconstruction map online with analog forecasting methods.

In the online stage, for a new observation  $y_k$ , we firstly estimate  $p(y_k|Y_k)$  with adaptive EnKF. Then the samples of  $\mathbf{y}_k$  are collected with  $\{\mathbf{y}_k^{a,1}, \dots, \mathbf{y}_k^{a,N}\}$  defined in (3.6). Given  $\mathbf{y}_k^{a,j}$ , we locate its  $M$  nearest neighbors within the set  $\mathcal{Y}$ :

$$\{\mathbf{y}_{k'}^{a,j}, \mathbf{y}_{k''}^{a,j}, \dots, \mathbf{y}_{k_M}^{a,j}\}.$$

The corresponding labels of these  $M$  neighbors in the set  $\mathcal{X}$  are  $\{x_{k'}, x_{k''}, \dots, x_{k_M}\}$ . We can utilize L-C operator or L-L operator to predict  $x_k^{a,j}$ , respectively. The selection of these operators mainly depends on the available computational resources and the complexity of the application [26]. The framework of KNN-Takens based EnKF is shown in Algorithm 3.

---

**Algorithm 3** KNN-Takens based EnKF

---

**Input:** historical trajectory  $\{x_k^{(i)}, y_k^{(i)}\}_{k=1}^T, i = 1, 2, \dots, M$ , new observation  $y_n$

**Output:** posterior  $p(x_n|Y_n)$

1: In the offline stage, denoise the observations with analog forecasting operators and construct the sets

$$\begin{aligned} \mathcal{Y} &= \{\mathbf{y}_d^{a,(1)}, \dots, \mathbf{y}_T^{a,(1)}, \dots, \mathbf{y}_d^{a,(M)}, \dots, \mathbf{y}_T^{a,(M)}\}, \\ \mathcal{X} &= \{x_d^{(1)}, \dots, x_T^{(1)}, \dots, x_d^{(M)}, \dots, x_T^{(M)}\}. \end{aligned}$$

2: In the online stage, estimate  $p(y_n|Y_n)$  with adaptive EnKF and estimate  $p(\mathbf{y}_n|Y_n)$ .

3: For each sample  $\mathbf{y}_n^{a,j}$ , locate its  $M$  nearest neighbors and utilize the analog forecasting operator to estimate  $x_n^{a,j}$ . The posterior distribution of  $x_n$  is approximated by

$$p(x_n|Y_n) \approx \frac{1}{N} \sum_{j=1}^N \delta_{x_n^{a,j}}(x_n).$$


---

## 5 Numerical results

In this section, we implement some numerical examples to illustrate the performance of DMD-T EnKF and KNN-T EnKF. In Section 5.1, we consider a pendulum model and estimate the overall model state from the partial and noisy observation by DMD-T EnKF.

In Section 5.2, we consider a stochastic model for topographic mean flow. In Section 5.3, KNN-T EnKF is applied to a Lorenz 63 model. In Section 5.4, we consider an example for Allen-Cahn equation with partial observations using DMD-T EnKF. To evaluate the performance of online estimation, we utilize the following metrics:

$$\text{RMSE} = \sqrt{\frac{1}{nT} \sum_{k=1}^T \|x_k - x_k^a\|_2^2},$$

$$\text{Spread} = \sqrt{\frac{1}{nT} \sum_{k=1}^T \text{Tr}(P_k^a)},$$

where  $k$  denotes the time index and  $n$  is the dimensionality of  $x_k$ .  $x_k^a$  and  $P_k^a$  represents the posterior mean and covariance of the model state, respectively.

## 5.1 Pendulum Model

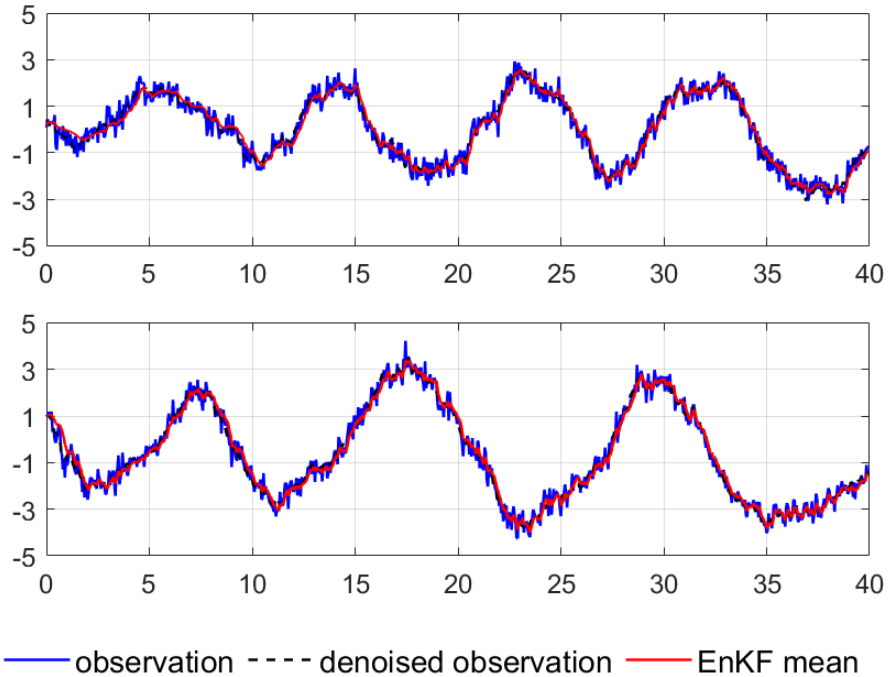


Figure 5.3: The posterior mean  $\hat{y}_k^a$  (red), the denoised observation (black dashed), the observation (blue) for the historical trajectories. We calculate  $K^{y,(0)}$  with noisy snapshots and update the matrix  $K^{y,(1)}$  with the posterior mean  $\hat{y}_k^a$ . The  $l^2$  norm of  $K^{y,(0)} - K^y$  and  $K^{y,(1)} - K^y$  are 0.1058 and 0.0126, respectively.

In this subsection, we consider the pendulum model with the state vector  $x_k = [\omega_k, \phi_k]^T$ , which incorporates the angular velocity  $\omega_k$  and the angle  $\phi_k$ . Suppose that the evolution

process is influenced by a random noise, then the transition model are governed by the following equation,

$$\begin{cases} \frac{\partial \omega}{\partial t} = -\frac{g}{l} \sin(\phi) + \sigma_1 \frac{dW_1}{dt}, \\ \frac{\partial \phi}{\partial t} = \omega + \sigma_2 \frac{dW_2}{dt}, \end{cases}$$

where  $g$  denotes the gravitational acceleration with a constant value of  $9.8 [m/sec^2]$ , and  $l$  represents the length of the pendulum's string and is set as  $l = 20$ . The continuous equation is discretized into a discrete-time system using Euler-Maruyama's method. The model can be expressed as

$$\begin{cases} \omega_{k+1} = \omega_k - \Delta_t \frac{g}{l} \sin(\phi_k) + \sigma_1 \xi_{1,k} \\ \phi_{k+1} = \phi_k + \Delta_t \omega_k + \sigma_2 \xi_{2,k}, \end{cases}$$

where  $\Delta t = 0.05$  and  $\xi_{1,k}, \xi_{2,k} \sim N(0, 1)$ , with noise variances  $\sigma_1^2 = \sigma_2^2 = 0.002$ . Additionally, the observation function is defined as

$$y_k = \phi_k + \eta_k,$$

where  $\eta_k \sim N(0, R)$  and  $R = 0.1$ . The historical trajectories consist of  $\{x_k^{(i)}, y_k^{(i)}\}_{k=1}^{800}$ ,  $i = 1, 2, \dots, 40$ . In the offline stage, the surrogate model  $K^y$  and the reconstruction map  $F$  is constructed by Algorithm 1. We calculate  $K^{y,(0)}$  with noisy snapshots and update the matrix  $K^{y,(1)}$  with the posterior mean  $\hat{y}_k^a$ . The  $l^2$  norm of  $K^{y,(0)} - K^y$  and  $K^{y,(1)} - K^y$  are 0.1058 and 0.0126, respectively. We select two historical trajectories. The posterior mean  $\hat{y}_k^a$  is showed in Fig. 5.3. It illustrates that the posterior mean  $\hat{y}_k^a$  can track the truth  $\hat{y}_k$ , achieving noise reduction. Additionally, the posterior mean  $\hat{y}_k^a$  can provide more accurate estimates of the transition model. After that, we set the delay coordinate vector  $\mathbf{y}_k$  with different lengths  $d = 2, 5, 10, 15$ . The reconstruction map is learned using the dataset  $\{x_k^{(i)}, \mathbf{y}_k^{(i),a}\}_{k=1}^{800}$ .

In the online stage, we utilize test data comprised of  $\{y_k\}_{k=1}^{1000}$  with different initial value to test the proxy model. The posterior mean  $x_k^a$  of test data is illustrated in Fig. 5.4. Setting  $d = 10$ , the posterior mean  $x_k^a$  is able to track the true trajectory and the truth falls within the confidence interval. The estimation of  $\phi_k$  is more accurate and exhibits less uncertainty than that of  $\omega_k$ . This discrepancy is attributed to the observation operator only containing information related to  $\phi_k$ . From Fig. 5.4(b), as  $d$  increases, the posterior mean  $\omega_k^a$  gradually approaches the truth value.

Fig. 5.5 shows the filtering distribution  $p(x_k|Y_k)$  of test data through kernel density estimation (KDE), where the horizontal axis represents  $\omega_k$  and the vertical axis represents  $\phi_k$ . It can be observed that the MAP estimate by DMD-T based EnKF is consistent with that of EnKF. The posterior distributions by DMD-T EnKF also exhibit a similar pattern to those of EnKF.

To explore the impact of the time-delay length  $d$ , we compute the relative errors and spreads of NNs and L-C operator. We plot the errors in Fig. 5.6 and see that the relative errors decrease as  $d$  increases. The relative error of  $\phi_k$  is not strongly correlated with the length  $d$  because the current observation has contained the complete information of  $\phi_k$ . While the relative error of  $\omega_k$  exhibits highly correlation with  $d$  and an increase of  $d$  leads to better estimation accuracy. Furthermore, the spreads decrease with increase of  $d$ . This may

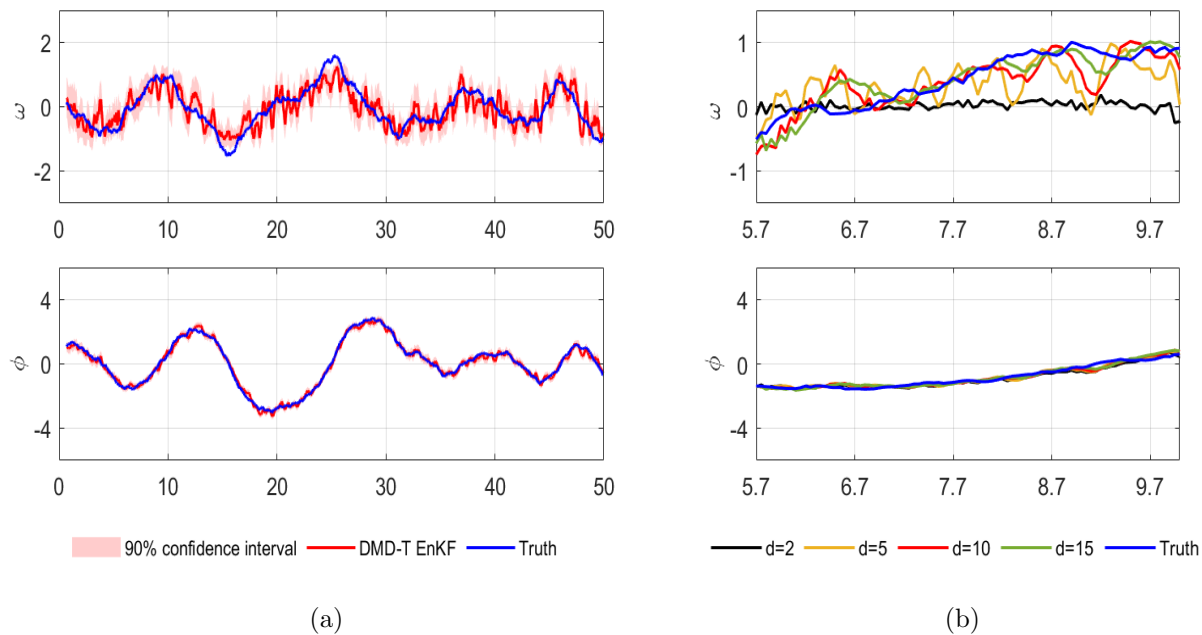


Figure 5.4: (a) The posterior mean  $x_k^a$  of test data by DMD-T EnKF when  $d = 10$ . (b) The posterior mean  $x_k^a$  of test data for different lengths  $d = 2, 5, 10, 15$  in the time window  $[5.7, 9.7]$ .

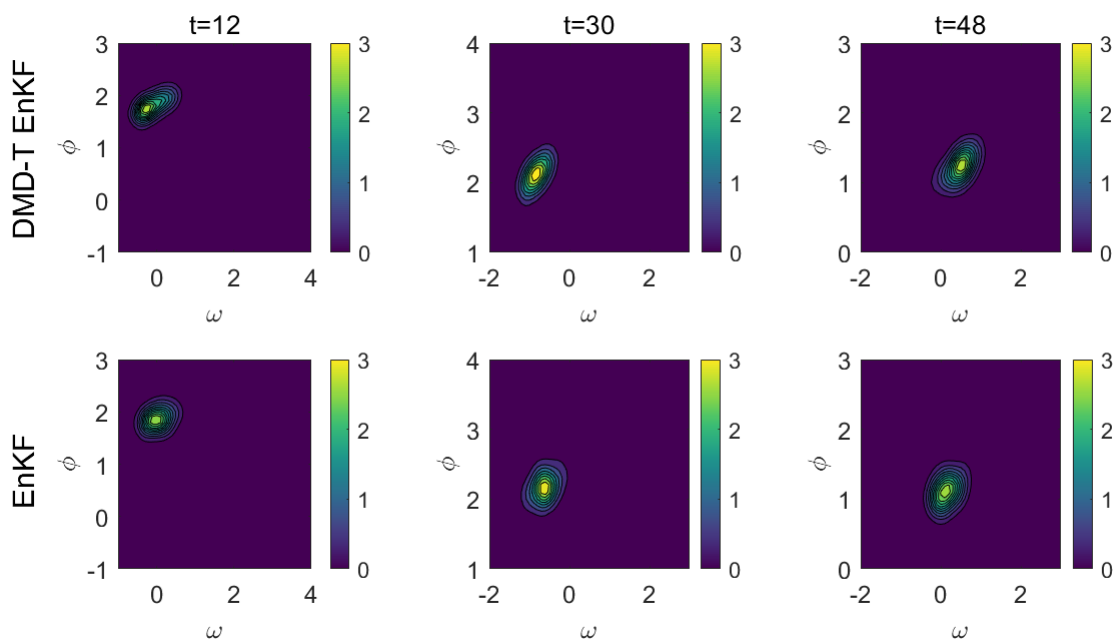


Figure 5.5: The filtering distribution  $p(x_k|Y_k)$  of test data at time points  $t = 12, 30, 48$  compared to EnKF ( $d = 10$ ). The horizontal axis represents  $\omega$ , and the vertical axis represents  $\phi$  estimated through KDE with the same bandwidth in two methods.

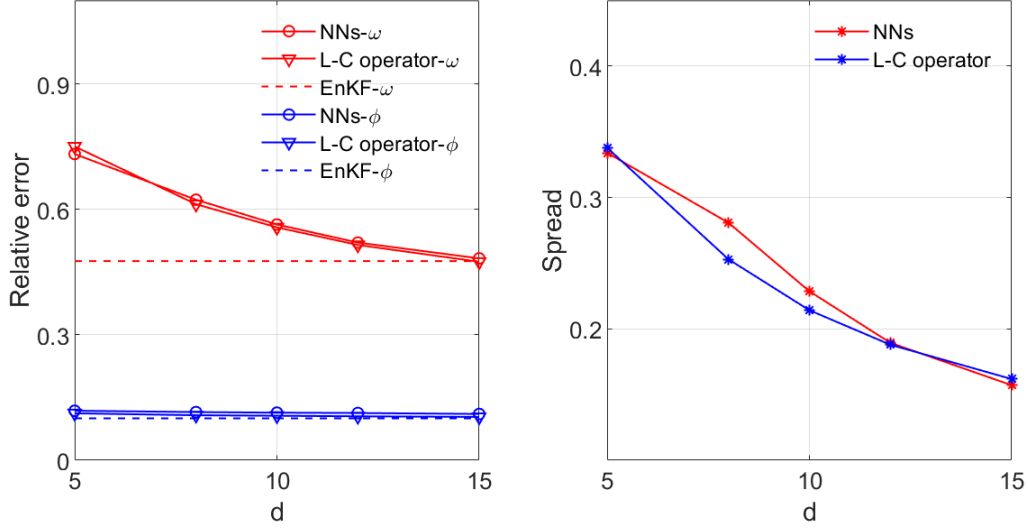


Figure 5.6: The relative errors and spreads with different modeling methods for the reconstruction map: NNs, L-C operator.

be due to the increased input dimension, which makes the reconstruction map more robust. With different modeling methods for the reconstruction map, the difference of NNs and L-C operator is not significant. When the model state dimension is low, nonparametric methods can be utilized to estimate  $x_k$  without the explicit learning of the map  $F$ .

## 5.2 A stochastic model

In this subsection, we consider a stringent paradigm model for topographic mean flow interaction, which is a kind of physics constrained multi-level regression models [29, 30]. With a specific choice of coefficients, the system can be expressed as follows:

$$dx = (Lx - Dx + B(x, x))dt + \sigma\Gamma dW, \quad (5.8)$$

where  $x = (u, v, w)^T$ ,  $B(x, x) = (0, auw, -auw)^T$ ,  $dW = (dW_1, dW_2)^T$ ,

$$L = \begin{pmatrix} 0 & \omega & 0 \\ -2\omega & 0 & -\beta \\ 0 & \beta & 0 \end{pmatrix}, \quad D = \begin{pmatrix} 0 & 0 & 0 \\ 0 & \gamma & 0 \\ 0 & 0 & \gamma \end{pmatrix}, \quad \Gamma = \begin{pmatrix} 0 & 0 \\ 1 & 0 \\ 0 & 1 \end{pmatrix}.$$

This form is similar to the Charney and DeVore model for nonlinear regime behavior without dissipation and forcing [29, 30]. We numerically discretize the continuous model with the Euler-Maruyama scheme as follows:

$$x_{i+1} = x_i + \delta t(Lx_i - Dx_i + B(x_i, x_i)) + \sigma\sqrt{\delta t}\Gamma\Delta W_{i+1}.$$

where  $\Delta W_{i+1} \sim N(0, I_2)$ . The parameters are assigned as  $\omega = 3/4, \gamma = 1/2, \beta = 1, a = 1, \sigma = 1/\sqrt{2}$  and  $\delta t = 0.1$ . Assume the noisy observation are available from the observation function

$$y_i = h(x_i) + \eta_i,$$

where  $\eta_i \sim N(0, R)$ . The functional form of  $h$  is specified as:

$$h = \begin{pmatrix} u + v \\ 2w \end{pmatrix}, \quad R = \begin{pmatrix} r & 0 \\ 0 & r \end{pmatrix},$$

where  $r = 0.1$ .

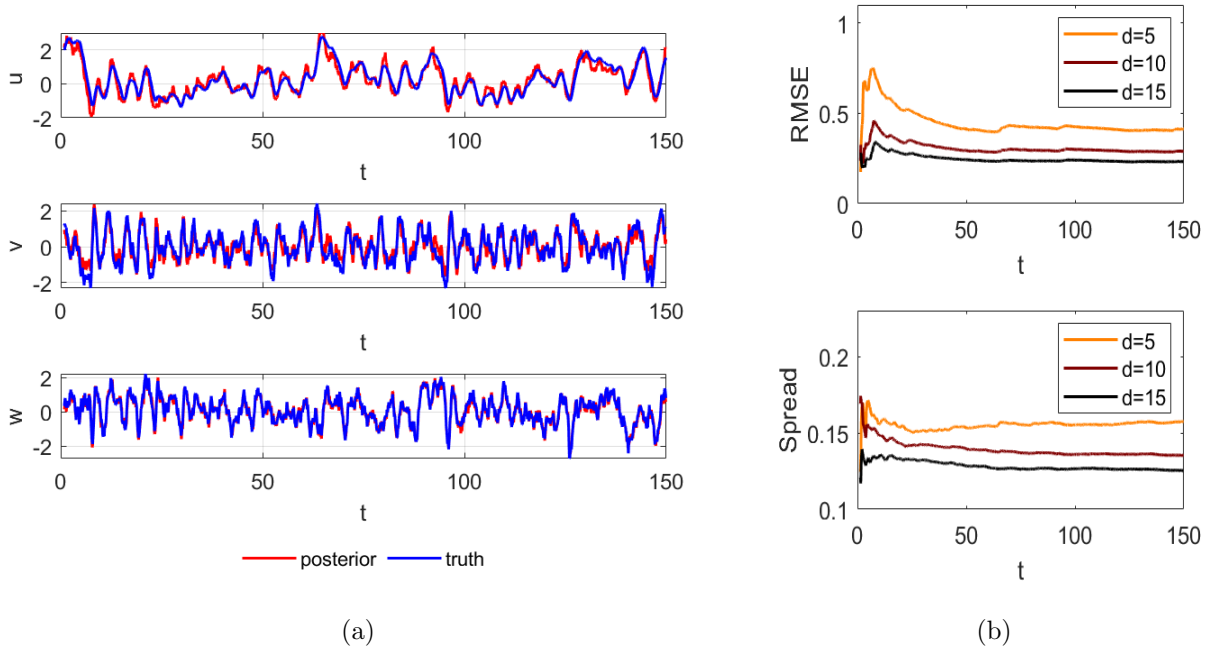


Figure 5.7: (a) The posterior mean  $x_k^a$  of test data with DMD-T EnKF when  $d = 10$ . (b) RMSEs and spreads of test data with different lengths  $d = 5, 10, 15$ .

	$K^{y,(0)}$	$K^{y,(1)}$	$K^{y,(2)}$	$K^{y,(3)}$
error( $l^2$ )	0.059999	0.018666	0.015302	0.015457

Table 1: the  $l^2$  error between  $K^{y,(t)}$  and  $K^y$ ,  $t = 0, 1, 2, 3$ .

Without the underlying dynamics, our aim is to construct the surrogate model for online estimation. The historical trajectories is composed of  $\{x_k^{(i)}, y_k^{(i)}\}_{k=1}^{500}$ ,  $i = 1, \dots, 20$ . Firstly, we construct the surrogate model with Algorithm 1. We repeat EnKF-DMD three times to estimate the DMD matrix  $K^y$  and the denoised observation  $\hat{y}$ . The  $l^2$  error of  $K^{y,(t)} - K^y$  is in Table 1. We observe that the iteration process can effectively reduce the  $l^2$  error between the estimated value and the truth value. This improvement can be explained from the perspective of the EM framework.

Then we set the delay coordinate vector  $\mathbf{y}_k = \{\hat{y}_k, \dots, \hat{y}_{k-d+1}\}$  with different time-delay lengths  $d = 5, 10, 15$ . We test the proxy model with new observation  $\{y_1, y_2, \dots, y_{1500}\}$  generated from different initial value. The posterior mean  $x_k^a$  of the test data is displayed in Fig. 5.7. The posterior mean can accurately track the truth. We observe that the estimation

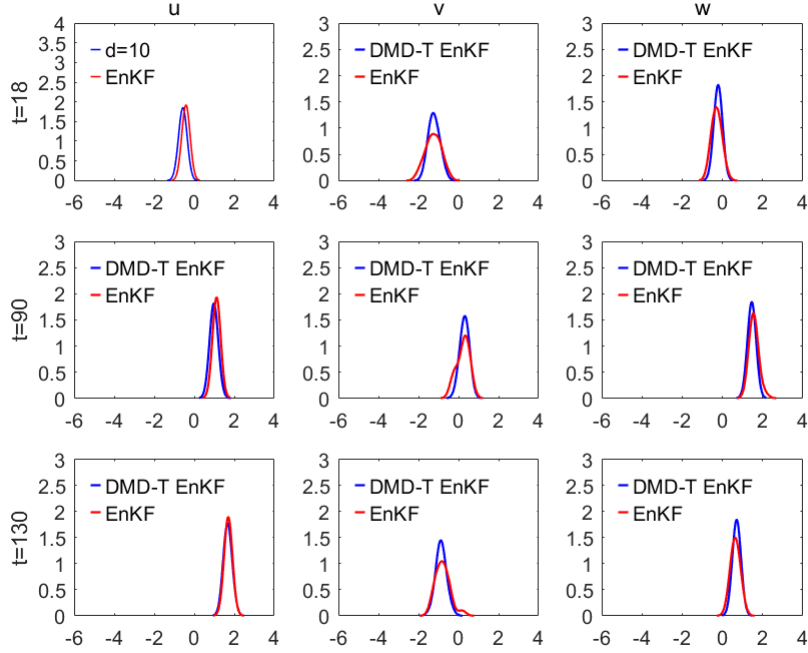


Figure 5.8: The marginal distribution of  $p(x_k|Y_k)$  estimated at time points  $t = 18, 90, 130$  compared to EnKF ( $d = 10$ ). The horizontal axis represents the value of variables, and the vertical axis represents the probability density estimated through KDE with the same bandwidth in two methods.

of  $w$  achieves better accuracy than other variables, due to the observation function containing complete information of  $w$ . Additionally, RMSEs and spreads decrease with increase of  $d$ . We plot marginal distribution of the three variables at  $t = 15, 90, 130$  in Fig. 5.8. The horizontal axis represents the value of variables, and the vertical axis represents the probability density estimated through KDE. It can be observed that the distribution estimated by DMD-T EnKF is very close to the distribution by EnKF.

To explore the sensitivity with different noise levels, we compute RMSEs and spreads compared to EnKF for  $\gamma = 0.1, 0.15, 0.2, 0.25, 0.3$ . The result is listed in Table 2. With the increase of noise magnitude, the RMSE increase rate of DMD-T EnKF remains approximately 4%, but the standard EnKF has 10%. This indicates that our proposed method remains effective under high noise magnitude conditions. Additionally, the spreads by DMD-T EnKF are smaller than those by EnKF. Unlike the standard EnKF, which provides prior information in the state space, DMD-T EnKF provides the prior information in the denoised observation space. The uncertainty of  $x_k$  depends on the uncertainty of  $\mathbf{y}_k$ . The decrease in uncertainty may be attributed to the robustness of the reconstruction map, which is trained with NNs.

noise magnitude	DMD-T EnKF		EnKF	
	RMSE	Spread	RMSE	Spread
0.1	0.291055	0.135308	0.184065	0.17918
0.15	0.303017	0.156167	0.214888	0.209518
0.2	0.319642	0.176229	0.238832	0.233021
0.25	0.330295	0.188462	0.258612	0.252394
0.3	0.335907	0.201737	0.275561	0.268970

Table 2: RMSEs and spreads of test data with different noise magnitude  $\gamma$  ( $d=10$ ).

### 5.3 Lorenz 63

In this section, we consider a chaotic system, which is explored by Lorenz for atmosphere convection in 1963. This Lorenz model exhibits high sensitivity to initial conditions and has chaotic characteristics. The model is described by a coupled nonlinear ordinary differential equations with an additive noise. The solution, denoted as  $v = (v_1, v_2, v_3) \in \mathbb{R}^3$ , satisfies

$$\begin{cases} \frac{dv_1}{dt} = a(v_2 - v_1) + \gamma_1 \frac{dW_1}{dt}, \\ \frac{dv_2}{dt} = -av_1 - v_2 - v_1v_3 + \gamma_2 \frac{dW_2}{dt}, \\ \frac{dv_3}{dt} = v_1v_2 - bv_3 - b(r + a) + \gamma_3 \frac{dW_3}{dt}. \end{cases}$$

The parameter values are assigned as  $(a, b, r) = (10, \frac{8}{3}, 28)$  and  $\gamma_1 = \gamma_2 = \gamma_3 = 0.05$ .

We can solve this continuous system with Euler-Maruyama scheme, where  $\delta_t = 0.01$ . It is assumed that noisy observation can be obtained through an observation function, which satisfies

$$y_k = h(v_k) + \eta_k,$$

where  $\eta_k \sim \mathcal{N}(0, \sigma^2)$ ,  $\sigma^2 = 2$ . The historical trajectories is comprised of  $\{x_k^{(i)}, y_k^{(i)}\}_{k=1}^{200}$ ,  $i = 1, \dots, 30$ . Algorithm 3 is employed for online estimation with nonparametric time series prediction methods. We locate  $N = 100$  nearest neighbors for analog forecasting. The delay coordinate vectors  $\mathbf{y}_k$  is formed with the length  $d = 20$ . The set of delay coordinate vectors  $\mathcal{Y}$  with the ensemble of successors  $\mathcal{X}$  is assigned as training data for the nonparametric online estimation.

Suppose an observation operator is given by  $h_1(v) = v_1 + v_2 + v_3$ , which includes only partial information about  $v$ . The surrogate model is constructed with Algorithm 3 and we utilize new observation  $\{y_k\}_{k=1}^{700}$  to test the proxy model. We estimate the filtering distribution  $p(v_k|Y_k)$  using KNN-T EnKF based on L-C operator and L-L operator, respectively. The result is shown in Fig. 5.9. It illustrates that our method can track the truth and effectively estimate the chaotic attractors. We can find that the estimation accuracy of L-L operator is higher than L-C operator. The L-L operator is semi-parametric with a locally weighed linear regression, while L-C operator is purely parametric relying on the training data. The metric spread measures the uncertainty inherent in samples  $x_k^{a,i}$ . The spread of L-L operator is larger than that of L-C operator. It leads to a big dispersion of prior ensembles by the posterior ensembles, with the transition model learned by L-L operator in the observation space.

Fig. 5.10 shows a comparison of filtering distribution with KDE by L-C operator, L-L operator, EnKF and the ground truth when  $t = 1.4, 4, 5.5$ . Compared to standard EnKF,

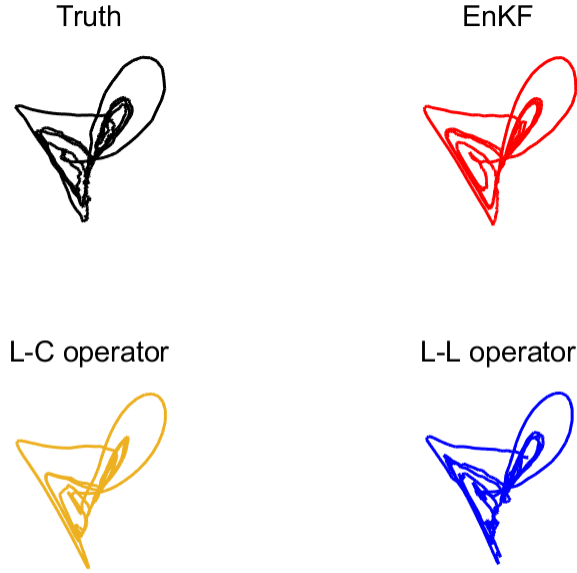


Figure 5.9: The posterior mean  $v_k^a$  of test data with KNN-T EnKF. Two different operators are utilized for the transition model and the reconstruction map: L-C operator and L-L operator, respectively. We compute the two metrics with different operators:  $\text{RMSE}_{\text{L-C}} = 2.9591$ ,  $\text{RMSE}_{\text{L-L}} = 2.2205$  and  $\text{spread}_{\text{L-C}} = 0.3719$ ,  $\text{spread}_{\text{L-L}} = 1.0703$ .

the two operators can both provide relatively accurate MAP estimations that are close to the ground truth. Our method estimates the uncertainty of distribution in the delay observation space instead of the original space. The distribution estimated by L-L operator will be more dispersed than L-C operator with respect to the larger spread and sensitivity of linear regression. Due to the nonlinearity of map  $F$ , the distribution exhibits stronger non-Gaussian characteristics.

To explore the impact of different observation functions, we suppose that new observation operator  $h_2$  satisfies

$$h_2(v) = \begin{pmatrix} v_1 + v_2 + v_3 \\ v_3 \end{pmatrix}.$$

We calculate RMSEs and spreads for two analog forecasting operators with different observation function  $h_1$  and  $h_2$ . The trend of RMSE and spread with regard to  $d$  is described in Fig. 5.11. The observation's dimension of  $h_2$  is twice that of  $h_1$ . So we establish the time-delay length of  $h_2$  to be half that of  $h_1$ , which can ensure the same dimension of  $\mathbf{y}_k$  for two observation functions. From Fig. 5.11, RMSEs and spreads are expected to decrease as  $d$  increases, attributed to the augmented information encapsulated within the delay coordinate vectors. If  $d$  is too small, the information derived from  $\mathbf{y}_k$  may be inadequate for estimating the chaotic attractors. Under a fixed dimension of  $\mathbf{y}_k$ , it becomes evident that the estimation of  $h_2$  yields better accuracy compared to  $h_1$ . It is rational to assert that

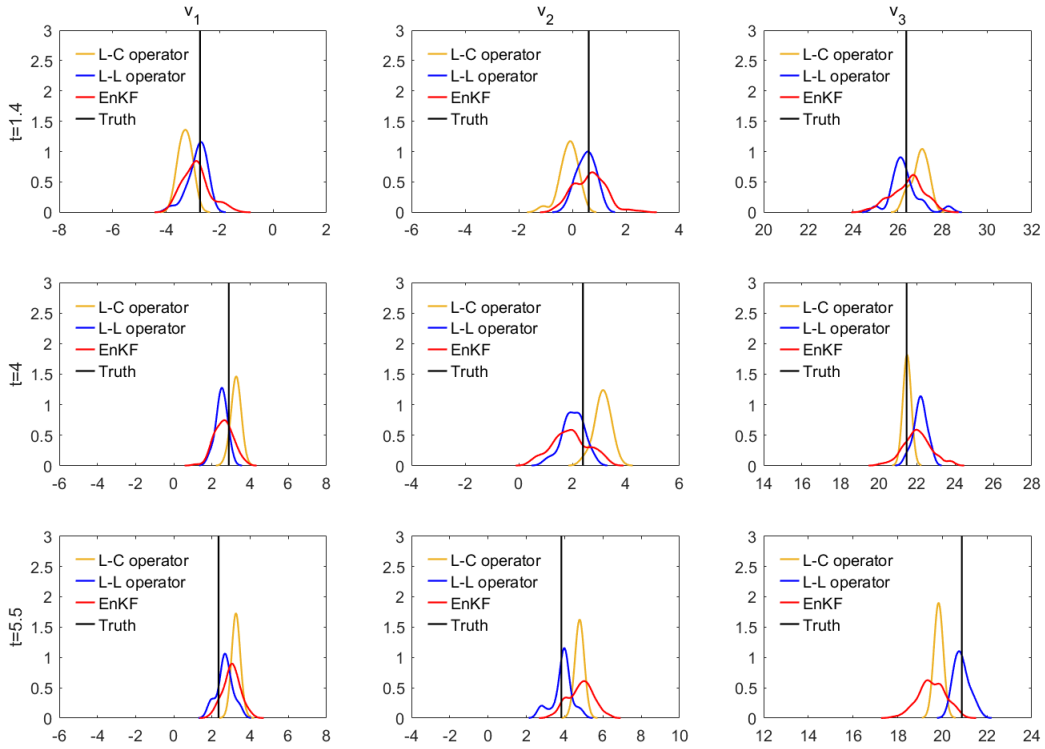


Figure 5.10: The marginal distribution of  $p(v_k|Y_k)$  estimated at time points  $t = 1.4, 4, 5.5$  compared to EnKF ( $d = 10$ ). The horizontal axis represents the value of variables, and the vertical axis represents the probability density estimated through KDE with the same bandwidth among three methods.

$h_2$  contains information pertaining to  $v_3$ , whereas  $h_1$  encompasses only partial information regarding the sum of three components in  $v$ . The estimation accuracy of L-L operator is larger than that of L-C operator and provides larger estimation uncertainty.

## 5.4 Allen-Cahn equation

Allen-Cahn equation has been widely used for phase transitions and interfacial dynamics in materials science. Initially proposed by Allen and Cahn, this equation was introduced to describe the motion of anti-phase boundaries within crystalline solids. It has found extensive application in various domains including crystal growth, phase transitions, image analysis, grain growth, and numerous other areas [31, 32].

In this section, we consider the one-dimensional Allen-Cahn equation

$$\begin{cases} \frac{\partial u}{\partial t} = \epsilon \frac{\partial^2 u}{\partial x^2} - \theta(u^3 - u);, \\ u(-1, t) = u(1, t), \quad u_x(-1, t) = u_x(1, t) \\ u(x, 0) = g(x), \end{cases}$$

where  $x \in [-1, 1], t \in [0, 1]$ . The parameters are set as  $\epsilon = 0.0001, \theta = 5$ . We employ

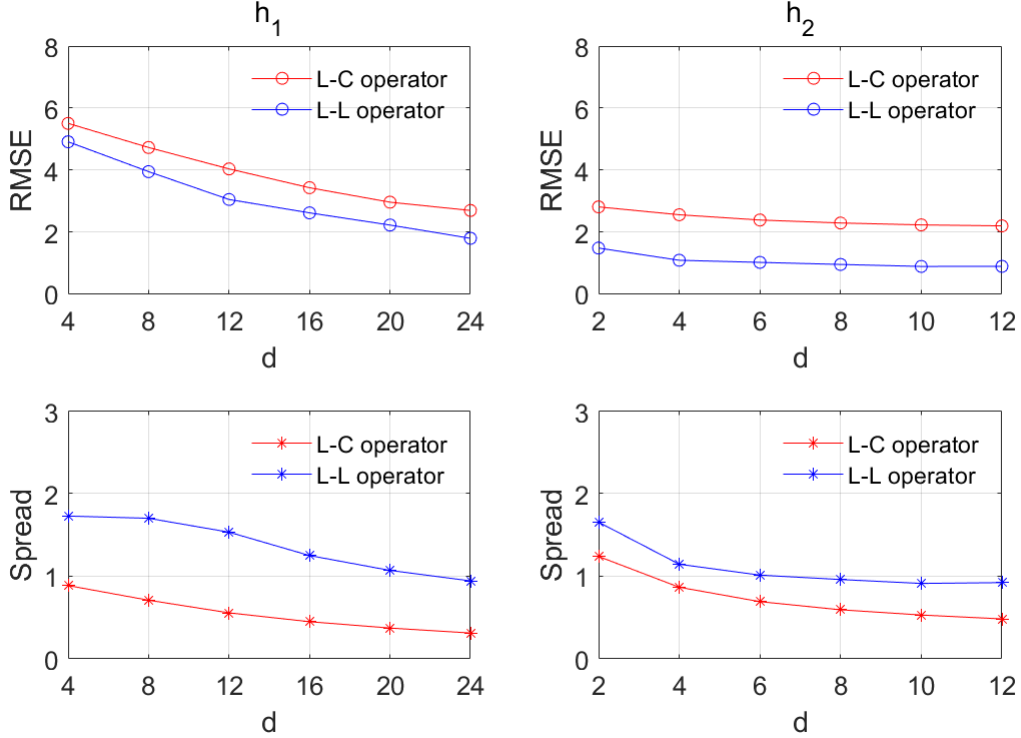


Figure 5.11: RMSEs and spreads with two analog forecasting operators for different observation functions  $h_1$  and  $h_2$ .

numerical discretization techniques, utilizing the temporal Crank-Nicolson method for time discretization and a second-order central difference scheme for spatial discretization. The spatial domain  $[-1, 1]$  is discretized using a finite grid with a spatial increment of  $\Delta x = 1/50$ , while the temporal domain  $[0, 1]$  is discretized with a time step of  $\Delta t = 1/500$ . We get a reference solution by employing the finite element method across all grid points.

Consider that the observation of this equation is accessible through an observation function

$$y = h(u) + \eta,$$

where  $\eta \sim \mathcal{N}(0, \sigma I)$ ,  $\sigma = 0.1$ . We assume  $h$  contains only the first 20 components of  $u$ , which satisfies

$$h(u) = u_{1:20}.$$

The historical data consists of  $\{u_k^{(i)}, y_k^{(i)}\}_{k=1}^{501}$ ,  $i = 1, \dots, 10$  initialized with different initial conditions  $u(x, 0)$ . Algorithm 1 is utilized to learn the proxy model with historical data. The time-delay length is  $d = 3$ . We employ the test data  $\{y_k\}_{k=1}^{501}$ , derived from the solution with initial conditions  $u(x, 0) = x^2 \cos(\pi x)$ , to examine the model's performance. Fig. 5.12 depicts the posterior mean  $u_k^a$  for the test data using DMD-T based EnKF and EnKF. We observe that the model state  $u_k$  estimated by the proposed method demonstrates symmetry about the spatial axis  $x = 0$ , aligning with the expected characteristics of the reference solution. The reason may be that the map  $F$  is learned from historical data and will preserve spatial

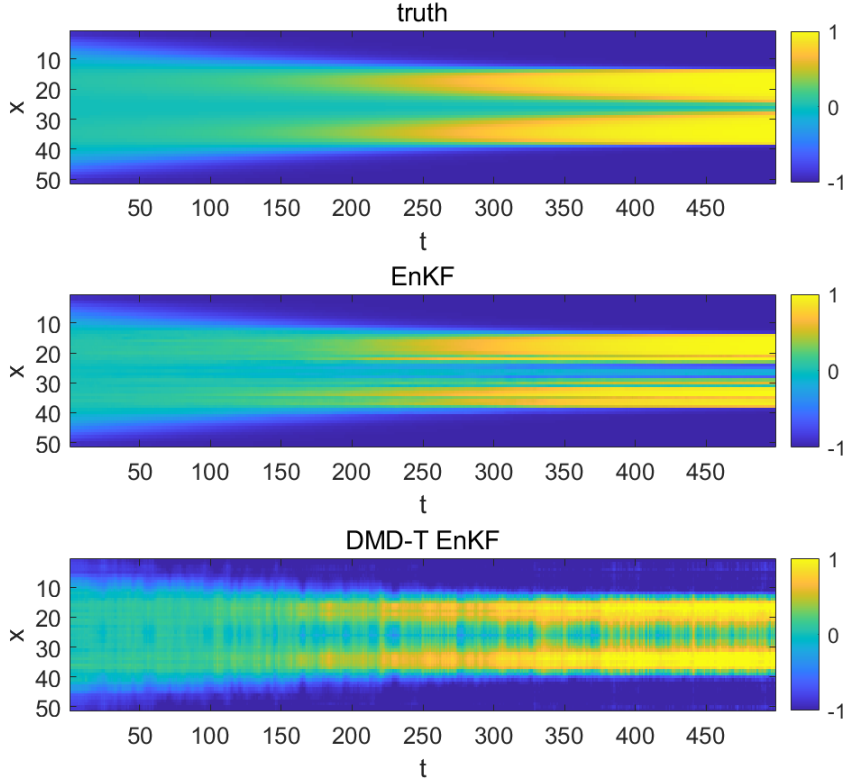


Figure 5.12: The posterior mean  $u_k^a$  of test data using DMD-T EnKF and EnKF.

symmetry. In contrast, the model state estimated by EnKF will be influenced by model error, resulting in the loss of this symmetry.

We describe the filtering distribution  $p(u_k|Y_k)$  for the test data through KDE in Fig. 5.13. The confidence intervals of  $u_k$  estimated by the proposed method keep symmetric about the spatial axis  $x = 0$  due to the characteristics of  $F$ . In contrast, with EnKF, the first 20 components are estimated more accurately due to the availability of observation containing information pertaining to these components. The remaining components, which lack observational data, are estimated with higher uncertainty. This indicates that our proposed approach, employing a data-driven method, retains the physical characteristics of the state space even when observational information is limited.

To investigate the impact of different operators, we estimate the model state  $u_k$  employing different operators for the reconstruction map: NNs, L-C operator and L-L operator in Fig. 5.14. The resulting RMSEs and spreads are presented in Table 3, which shows that NNs has the best accuracy and robustness. L-C operator, as a non-parametric approach, yields smoother estimations of the model state. In contrast, L-L operator exhibits strong sensitivity to small perturbations due to its use of weighted linear regression, resulting in more oscillatory estimations of the model state.

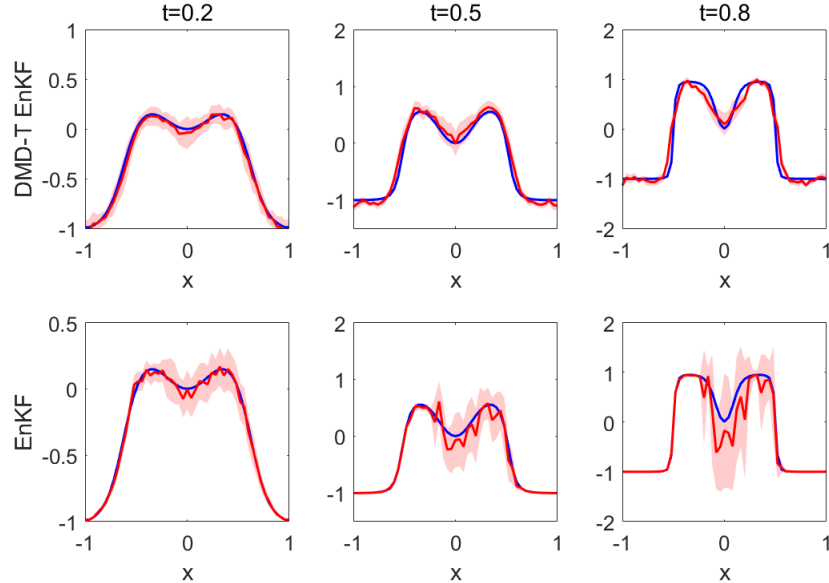


Figure 5.13: The filtering distribution of test data estimated through KDE at time points  $t = 0.2, 0.5, 0.8$ .

	Neural Networks	L-C operator	L-L operator	EnKF
RMSE	0.146922	0.181342	0.202467	0.177576
Spread	0.067872	0.067539	0.314727	0.178170

Table 3: RMSEs and spreads of test data by different operators for the reconstruction map: NNs, L-C operator and L-L operator.

## 6 Conclusions

In this paper, we presented DMD-T EnKF for online estimation without the underlying dynamics. In the offline stage, we constructed the transition model for observation and the reconstruction map. The process of estimating the transition model can be interpreted by the perspective of EM algorithm. Then the reconstruction map was learned with the embedding and its corresponding model state. In the online stage, we utilized the surrogate model to estimate the model state. Furthermore, we developed this framework with nonparametric time series prediction methods, namely KNN-T EnKF. The transition model and the reconstruction map has been estimated with analog forecasting methods, without learning the specific form. The numerical results showed that the proposed approach can use data pairs of the dynamical model and accurately approximate the filtering distribution. The stability and accuracy can be enhanced by Takens theorem.

## Aknowledge

L. Jiang acknowledges the support of NSFC 12271408.

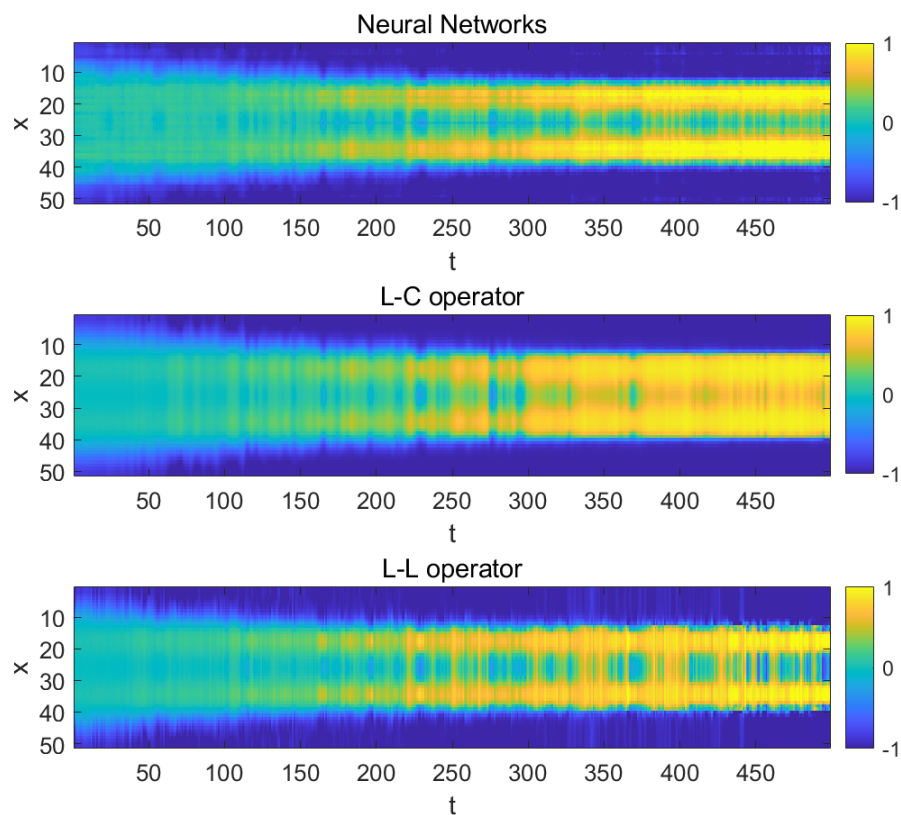


Figure 5.14: The posterior mean  $u_k^a$  of test data estimated with different operators for the reconstruction map: NNs, L-C operator and L-L operator.

**Conflict of interest statement:** The authors have no conflicts of interest to declare. All co-authors have seen and agree with the contents of the manuscript.

## References

- [1] K. Law, A. Stuart, K. Zygalakis, Data Assimilation: A Mathematical Introduction, Springer International Publishing, 2015.
- [2] A. Hauschild, O. Montenbruck, Kalman-filter-based GPS clock estimation for near real-time positioning, GPS Solutions 13 (2009) 173–182.
- [3] D. S. Oliver, A. C. Reynolds, N. Liu, Inverse Theory for Petroleum Reservoir Characterization and History Matching, Cambridge University Press, 2008.
- [4] E. Kalnay, Atmospheric Modeling, Data Assimilation and Predictability, Cambridge University Press, 2002.

- [5] R. E. Kalman, A New Approach to Linear Filtering and Prediction Problems, *Journal of Basic Engineering* 82 (1960) 35–45.
- [6] A. H. Jazwinski, *Stochastic processes and filtering theory*, Courier Corporation, 2007.
- [7] D. T. Kelly, K. J. Law, A. M. Stuart, Well-posedness and accuracy of the ensemble kalman filter in discrete and continuous time, *Nonlinearity* 27 (2014) 2579.
- [8] A. Doucet, A. M. Johansen, et al., A tutorial on particle filtering and smoothing: Fifteen years later, *Handbook of nonlinear filtering* 12 (2009) 3.
- [9] G. Revach, N. Shlezinger, X. Ni, A. L. Escoriza, R. J. Van Sloun, Y. C. Eldar, Kalmanet: Neural network aided kalman filtering for partially known dynamics, *IEEE Transactions on Signal Processing* 70 (2022) 1532–1547.
- [10] M. Bocquet, J. Brajard, A. Carrassi, L. Bertino, Bayesian inference of chaotic dynamics by merging data assimilation, machine learning and expectation-maximization, *Foundations of Data Science* 2 (2020) 55–80.
- [11] N. Liu, L. Jiang, Perron-frobenius operator filter for stochastic dynamical systems, *SIAM/ASA Journal on Uncertainty Quantification* 12 (2024) 182–211.
- [12] Y. Ba, L. Jiang, N. Ou, A two-stage ensemble kalman filter based on multiscale model reduction for inverse problems in time fractional diffusion-wave equations, *Journal of Computational Physics* 374 (2018) 300–330.
- [13] C. W. Rowley, I. Mezić, S. Bagheri, P. Schlatter, D. S. Henningson, Spectral analysis of nonlinear flows, *Journal of fluid mechanics* 641 (2009) 115–127.
- [14] P. J. Schmid, Dynamic mode decomposition of numerical and experimental data, *Journal of Fluid Mechanics* 656 (2010) 5–28.
- [15] J. N. Kutz, S. L. Brunton, B. W. Brunton, J. L. Proctor, *Dynamic mode decomposition: data-driven modeling of complex systems*, SIAM, 2016.
- [16] K. Champion, B. Lusch, J. N. Kutz, S. L. Brunton, Data-driven discovery of coordinates and governing equations, *Proceedings of the National Academy of Sciences* 116 (2019) 22445–22451.
- [17] S. A. Falconer, D. J. Lloyd, N. Santitissadeekorn, Combining dynamic mode decomposition with ensemble kalman filtering for tracking and forecasting, *Physica D: Nonlinear Phenomena* 449 (2023) 133741.
- [18] L. Jiang, N. Liu, Correcting noisy dynamic mode decomposition with kalman filters, *Journal of Computational Physics* 461 (2022) 111175.
- [19] F. Hamilton, T. Berry, T. Sauer, Ensemble kalman filtering without a model, *Physical Review X* 6 (1) (2016) 011021.

- [20] F. Takens, Detecting strange attractors in turbulence, in: *Dynamical Systems and Turbulence, Warwick 1980: proceedings of a symposium held at the University of Warwick 1979/80*, Springer, 2006, pp. 366–381.
- [21] E. R. Deyle, G. Sugihara, Generalized Theorems for Nonlinear State Space Reconstruction, *PLoS ONE* 6 (2011) e18295.
- [22] C. D. Young, M. D. Graham, Deep learning delay coordinate dynamics for chaotic attractors from partial observable data, *Physical Review E* 107 (2023) 034215.
- [23] T. Berry, T. Sauer, Adaptive ensemble kalman filtering of non-linear systems, *Tellus A: Dynamic Meteorology and Oceanography* 65 (2013) 20331.
- [24] T. Berry, J. Harlim, Variable bandwidth diffusion kernels, *Applied and Computational Harmonic Analysis* 40 (2016) 68–96.
- [25] C. G. Schroer, T. Sauer, E. Ott, J. A. Yorke, Predicting chaos most of the time from embeddings with self-intersections, *Physical Review Letters* 80 (1998) 1410.
- [26] R. Lguensat, P. Tandeo, P. Ailliot, M. Pulido, R. Fablet, The analog data assimilation, *Monthly Weather Review* 145 (2017) 4093–4107.
- [27] M. B. Kennel, R. Brown, H. D. Abarbanel, Determining embedding dimension for phase-space reconstruction using a geometrical construction, *Physical review A* 45 (1992) 3403.
- [28] S. P. Garcia, J. S. Almeida, Multivariate phase space reconstruction by nearest neighbor embedding with different time delays, *Physical Review E* 72 (2005) 027205.
- [29] J. Harlim, A. Mahdi, A. J. Majda, An ensemble kalman filter for statistical estimation of physics constrained nonlinear regression models, *Journal of Computational Physics* 257 (2014) 782–812.
- [30] J. G. Charney, J. G. DeVore, Multiple flow equilibria in the atmosphere and blocking, *Journal of Atmospheric Sciences* 36 (1979) 1205–1216.
- [31] J. W. Cahn, J. E. Hilliard, Free energy of a nonuniform system. i. interfacial free energy, *The Journal of chemical physics* 28 (1958) 258–267.
- [32] K. Poochinapan, B. Wongsaijai, Numerical analysis for solving allen-cahn equation in 1d and 2d based on higher-order compact structure-preserving difference scheme, *Applied Mathematics and Computation* 434 (2022) 127374.